eters, even for cases where the Rietveld method already underestimates it.

Conclusions

The conclusions which can be drawn from this study are as follows.

1. The values of the e.s.d.'s given by the Rietveld method are not reliable.

2. Introduction of off-diagonal terms in the weight matrix may give better values for the e.s.d.'s, but will in general be insufficient to ensure their reliability.

3. Reliable values of the e.s.d.'s can only be determined if the form of the dependence of the calculated intensities on the two different types of parameters is taken into account.

4. Of the methods considered in this paper only the SCRAP method will in general give reliable values for the e.s.d.'s of the structural parameters.

Postscript

Since the present paper was written a further paper discussing the Rietveld method has been published by Prince (1981). However, Prince's paper is misleading because, although he also shows that the model must be adequate on the basis of statistical tests, he assumes that this conflicts with the conclusions of Sakata & Cooper (1979). [The introduction also contains a misquotation from the paper by Sakata & Cooper (1979). These authors do not assert that the profile method (always) 'leads to a systematic underestimate of the uncertainties of the crystallographic parameters'. Indeed, the present paper shows that these uncertainties may also be overestimated in certain circumstances.]

In fact the majority of the discussion presented by Prince is in very close agreement with the analysis of Sakata & Cooper. The three statistics S_P^2, S_L^2 and S_R^2 defined by Prince's equations (9) to (11) are directly related to the quantities A_P^2, A_B^2 and A_S^2 defined by Sakata & Cooper. Thus the conclusion that the model is only correct if S_L^2/S_R^2 is unity is very similar to the relationship between A_B^2 and A_S^2 for which the e.s.d. values are reliable, as derived by Sakata & Cooper. However, it is also misleading to call S_R^2 the 'replication mean square', since measurement at different 2θ values cannot be considered as replication in the sense used by Draper & Smith (1966).

The papers by Prince and by Sakata & Cooper are thus in agreement that the Rietveld method cannot calculate the standard deviations correctly if the model does not fit adequately. However, examination of published results indicates that in general the model does not fit adequately on the basis of these statistical criteria, so that the Rietveld method will consequently give unreliable values for the e.s.d.'s.

References

CLARKE, C. P. & ROLLETT, J. S. (1982) *Acta Cryst.* Submitted.

COOPER, M. J., ROUSE, K. D. & SAKATA, M. (1981). *Z. Kristallogr.* **157**, 101–117.

DRAPER, N. R. & SMITH, H. (1966). *Applied Regression Analysis*, pp. 26–32. New York: Wiley.

PRINCE, E. (1981). *J. Appl. Cryst.* **14**, 157–159.

RIETVELD, H. M. (1967). *Acta Cryst.* **22**, 151–152.

RIETVELD, H. M. (1969). *J. Appl. Cryst.* **2**, 65–71.

ROLLETT, J. S. (1979). Private communication.

SAKATA, M. & COOPER, M. J. (1979). *J. Appl. Cryst.* **12**, 554–563.

Acta Cryst. (1982). A**38**, 269–274

One-Dimensional Antiphase Structure of $Au_{22}Mn_6$ Studied by High-Voltage, High-Resolution Electron Microscopy

BY K. HIRAGA AND M. HIRABAYASHI

The Research Institute for Iron, Steel and Other Metals, Tohoku University, Sendai 980, *Japan*

AND O. TERASAKI AND D. WATANABE

Department of Physics, Faculty of Science, Tohoku University, Sendai 980, *Japan*

(*Received* 29 *July* 1981; *accepted* 30 *October* 1981)

Abstract

Au–Mn alloys near the composition of 20% Mn have been investigated by the superstructure imaging technique using a 1 MV electron microscope. A new superstructure, $Au_{22}Mn_6$, was proposed directly from the high-resolution images. The structure is based on the Au_4Mn structure of Ni_4Mo ($D1a$) type and consists of parallel columns with a width of three Mn-atom rows, and the columns are separated by one-

0567-7394/82/020269-06$01.00

dimensional antiphase boundaries parallel to the (210) plane of the fundamental f.c.c. structure. Structural modulation and local disorder were also revealed at the atomic scale.

I. Introduction

Gold-rich Au–Mn alloys have been the subject of a number of investigations by high-resolution electron microscopy combined with selected-area electron diffraction (Amelinckx, 1978–9; Watanabe, 1979; Van Tendeloo, 1980). The current potentiality of high voltage, high-resolution electron microscopy (HVHREM) has made it possible to observe direct images of constituent atoms in ordered alloys. The HVHREM images which were interpretable straightforwardly in terms of the superstructure have been named superstructure images (Hiraga, Shindo & Hirabayashi, 1980, 1981). These images were formed by interference of many beams of the superlattice reflections with symmetrical incidence along a principal axis. The technique has been applied to the studies of Au–Mn alloys (Terasaki, Watanabe, Hiraga, Shindo & Hirabayashi, 1980). Recently we reported the direct determination of a hitherto undescribed superstructure $Au_{31}Mn_9$ from the superstructure images (Hiraga, Shindo, Hirabayashi, Terasaki & Watanabe, 1980, hereafter referred to as part I). The structure consists of square-shaped islands of the Au_4Mn structure of Ni_4Mo ($D1a$) type, and the islands are separated by two-dimensional antiphase boundaries ($2d$-APB). Further, we studied a two-dimensional antiphase structure ($2d$-APS) based on the structure of Al_3Ti ($D0_{22}$) type in the range 20–23 at.% Mn (Terasaki, Watanabe, Hiraga, Shindo & Hirabayashi, 1981, part II). In the course of successive HVHREM studies on the Au–Mn alloys, we found a new type of one-dimensional antiphase structure ($1d$-APS) based on the Au_4Mn structure of the $D1a$ type. The purpose of the present paper is to clarify the atomic arrangement of this structure and its related structural modulations by means of the superstructure imaging technique.

II. Experimental

Au–Mn alloys containing 19·5 and 20·7 at.% Mn were investigated with a 1 MV electron microscope. The specimens, prepared by the same method as used in parts I and II, were annealed at 573 K for 40–50 days; the annealing temperature was lower than that (673 K) used in part I. The superstructure images were taken with the symmetrical incidence parallel to the [001] direction.*

* Indices refer to the fundamental face-centered cubic structure throughout this paper.

In the micrographs presented below, the Mn-atom rows along the beam direction are seen as bright or dark dots depending on foil thickness and defocus condition. The images are interpreted on the basis of the one-to-one correspondence between the Mn-atom rows and the dots.

III. Results and discussion

The stable structure at 20 at.% Mn below 600 K is the Au_4Mn structure of the $D1a$ type (Watanabe, 1957). This structure is described by the space group $I4/m$ with two Mn atoms in $2(a)$ and eight Au atoms in $8(h)$ ($x = \frac{1}{4}$, $y = \frac{2}{5}$). The fundamental lattice vectors of the tetragonal superstructure are given by $\mathbf{A}_1 = (3\mathbf{a}_1 - \mathbf{a}_2)/2$, $\mathbf{A}_2 = (\mathbf{a}_1 + 3\mathbf{a}_2)/2$ and $\mathbf{C} = \mathbf{a}_3$, where $\mathbf{a}_1$, $\mathbf{a}_2$ and $\mathbf{a}_3$ are those of the basic f.c.c. lattice. Since $a(=a_1 = a_2 = a_3)$ is 4·0 Å, the unit-cell parameter A $(=A_1 = A_2)$ is $a\sqrt{10}/2 = 6{\cdot}3$ Å.

Fig. 1. shows a HVHREM image of the Au_4Mn structure of Au–19·5 at.% Mn annealed at 573 K for 48 days, together with the corresponding electron diffraction pattern and optical diffractogram. Bright dots in Fig. 1(a) align regularly on a square lattice. The one-to-one correspondence between the bright dots and the Mn-atom rows in the Au_4Mn structure has been proved from computer calculations by the

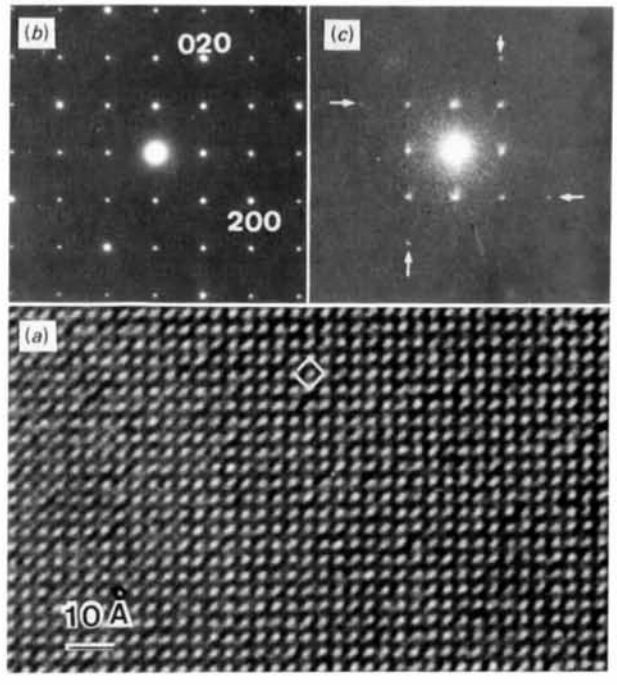

Fig. 1. (a) Superstructure image and (b) electron diffraction pattern of the Au_4Mn structure (19·5 at.% Mn). A square corresponds to the unit cell of $A = 6{\cdot}3$ Å. Arrows in the optical diffractogram (c) indicate the fundamental spots of type 200.

multislice method (Terasaki *et al.*, 1980). The closest distance between dots is about 4·5 Å which corresponds to $A/\sqrt{2}$. In the electron diffraction pattern of Fig. 1(*b*), a number of superlattice spots are distributed on a square net with the spacing $2a^*/\sqrt{5}$, and are indexed as $\frac{420}{33}0$, $\frac{260}{33}0$ *etc.* The optical diffractogram of Fig. 1(*c*) indicates that the superlattice reflections of $\frac{420}{33}0$ and $\frac{260}{33}0$ types are highly excited and contribute predominantly to the observed image.

Modulations of the Au_4Mn structure were found in the Au–20·7 at.% Mn alloy annealed at 573 K for 45 days. An antiphase boundary (APB) parallel to the (210) plane is seen in the image of Fig. 2; misalignments of the dot arrangement take place at the boundary indicated by vertical arrows. The pairs of bright dots at the boundary marked with small arrows align along the [100] direction with a distance of 4 Å. This suggests that the APB is of the second kind, or non-conservative, with a misalignment vector of (**a**/2) [011]. The APB of this type accommodates the excess Mn atoms over the stoichiometric composition Au_4Mn.

In fact, the APB's were observed more often in the 20·7 at.% Mn alloy than in the 19·5 at.% Mn alloy. The APB's tend to align regularly as shown in the region *b* of Fig. 3, whereas the region *a* is of the Au_4Mn-type structure containing no faults. The region *b* is composed of parallel columns with a width of three bright dots, and the misalignments occur at every fourth dot. The columns, which may be named three-dot columns, are arranged regularly, as marked with white lines. The superstructure of the region *b* is described as a 1*d*-APS based on the Au_4Mn structure; a parallelogram outlined in the image corresponds to a projection of the monoclinic unit cell.

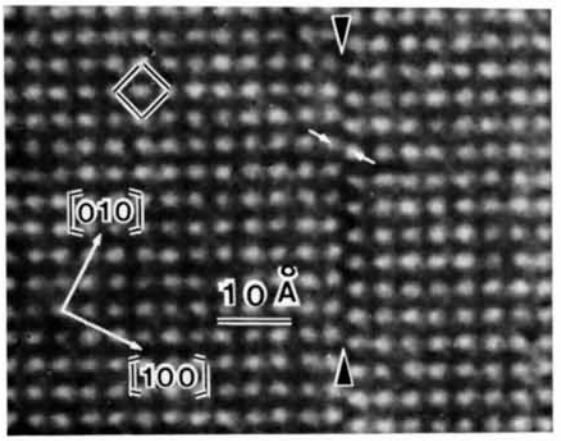

Fig. 2. Superstructure image showing an antiphase boundary in the Au_4Mn structure. Small arrows at the boundary indicate the closest Mn atom pairs at a distance of 4·0 Å along [100] (see Fig. 4).

The atomic arrangement in the monoclinic cell is readily proposed from the image, as illustrated in Fig. 4. The crystallographic parameters of this structure are listed in Table 1. Hereafter it is referred to as the $Au_{22}Mn_6$ structure since the unit cell contains 22 Au and 6 Mn atoms, corresponding to the composition 21·4 at.% Mn. It is seen in Fig. 4 that the pairs of Mn atoms in 4(*e*) ($z = 0$ or $\frac{1}{2}$) have an interatomic distance $a = 4{\cdot}0$ Å.

It is interesting to note that the superstructure image of the $Au_{22}Mn_6$ structure may be described in terms of one-dimensional concentration density waves of the Mn-atom rows of which the wave vector is parallel to the [$\bar{1}$30] direction. The bright dots in the region *b* of Fig. 3 align, on average, along the [310] direction or the *A* axis of the $Au_{22}Mn_6$ cell. This is clearly seen when the image is viewed obliquely along this direction. Contrarily, the concentration density waves in the Au_4Mn structure appear parallel to the [210] and [1$\bar{2}$0] directions.

The electron diffraction pattern inserted in Fig. 3 was obtained from a limited area of about 1000 Å in

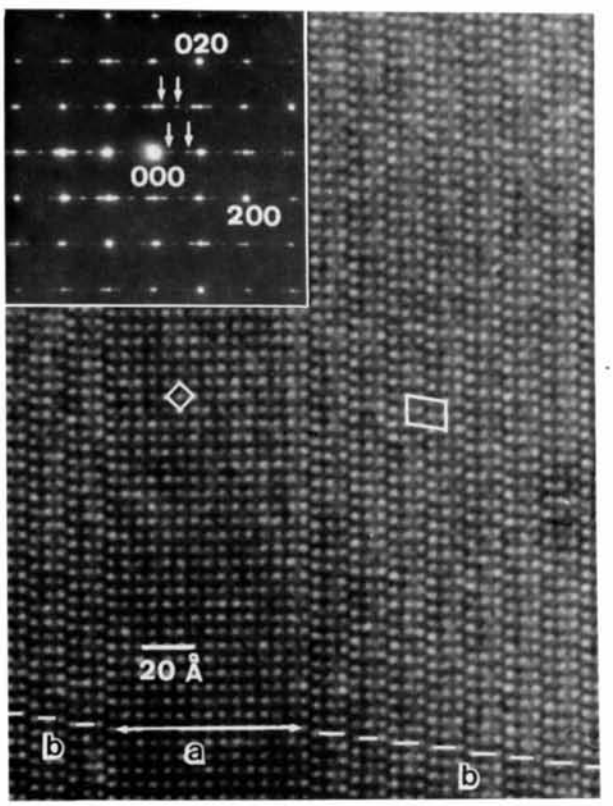

Fig. 3. Superstructure image of Au–20·7 at.% Mn, showing intergrowth of (*a*) the Au_4Mn structure and (*b*) the $Au_{22}Mn_6$ structure. In the region *b*, white lines aligned step-wise indicate the three-dot columns separated by APB's. Superstructure reflections of the $Au_{22}Mn_6$ structure are shown by arrows in the electron diffraction pattern.

diameter. This pattern shows strong superlattice reflections of the Au_4Mn structure and weak ones of the $Au_{22}Mn_6$ structure in addition to the fundamental reflections of the f.c.c. lattice. The observed intensity distributions agree well with those calculated kinematically for the respective superstructures. The characteristic feature of the diffraction pattern is diffuse streaks running parallel to the horizontal direction, which suggests irregular distributions of the APB's along the [210] direction. In fact, various kinds of structural modulations or irregularities are observed in the HVHREM images.

As an example, the image of Fig. 5 shows structural modulations and defects in the $Au_{22}Mn_6$ structure coexisting with the Au_4Mn structure. Near *A* at the upper right, there is a sequential alignment of the bright dots labeled as 33433; a column with the width of four dots is mixed with the three-dot columns. Near *B*, we can see two dark stripes indicated by small arrows, where the column width changes gradually from four dots to three dots along the vertical arrows. Large dark spots of butterfly-shaped contrast, *C*, are attributed to the local strain of dislocation loops which are formed by the clustering of point defects induced by 1 MV electron irradiation. This will be discussed later. The region *D* is enlarged in Fig. 6 to exhibit more clearly the structural modulations.

On the right of Fig. 6, there is a dark stripe corresponding to the APB between the three-dot

Table 1. *Superstructure of* $Au_{22}Mn_6$

Space group	$P2_1/b$ (No. 14), monoclinic
Unit-cell dimensions	$A = \sqrt{10}a = 12{\cdot}6$ Å, $B = \sqrt{5}a = 8{\cdot}9$ Å.
	$C = a = 4{\cdot}0$ Å, $\gamma = 81{\cdot}8°$
Unit-cell contents	22 Au atoms, 6 Mn atoms
Atomic positions	
2 Mn in 2(*a*)	$0,0,0;\ 0,\frac{1}{2},\frac{1}{2}$
4 Mn in 4(*e*)	$x,y,z;\ \bar{x},\frac{1}{2}-y,\frac{1}{2}+z;$
	$\bar{x},\bar{y},\bar{z};\ x,\frac{1}{2}+y,\frac{1}{2}-z$
	$x=\frac{4}{14}, y=\frac{1}{14}, z=\frac{1}{2}$
2 Au in 2(*b*)	$\frac{1}{2},0,0;\ \frac{1}{2},\frac{1}{2},\frac{1}{2}$
20 Au in 4(*e*)	$x=\frac{1}{4}, y=\frac{6}{14}, z=0;$
	$x=\frac{3}{14}, y=\frac{1}{4}, z=0;$
	$x=\frac{6}{14}, y=\frac{4}{14}, z=0;$
	$x=\frac{1}{14}, y=\frac{3}{14}, z=\frac{1}{2};$
	$x=\frac{4}{14}, y=\frac{2}{14}, z=\frac{1}{2}$

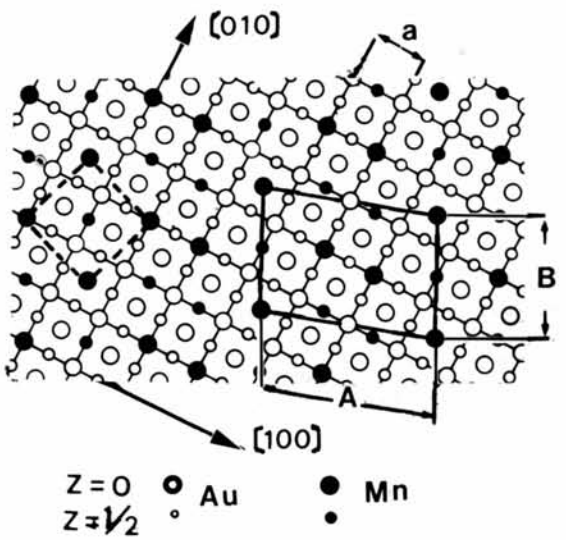

Fig. 4. Atomic arrangement of the $Au_{22}Mn_6$ structure projected along [001]. The dashed square corresponds to the unit cell of Au_4Mn.

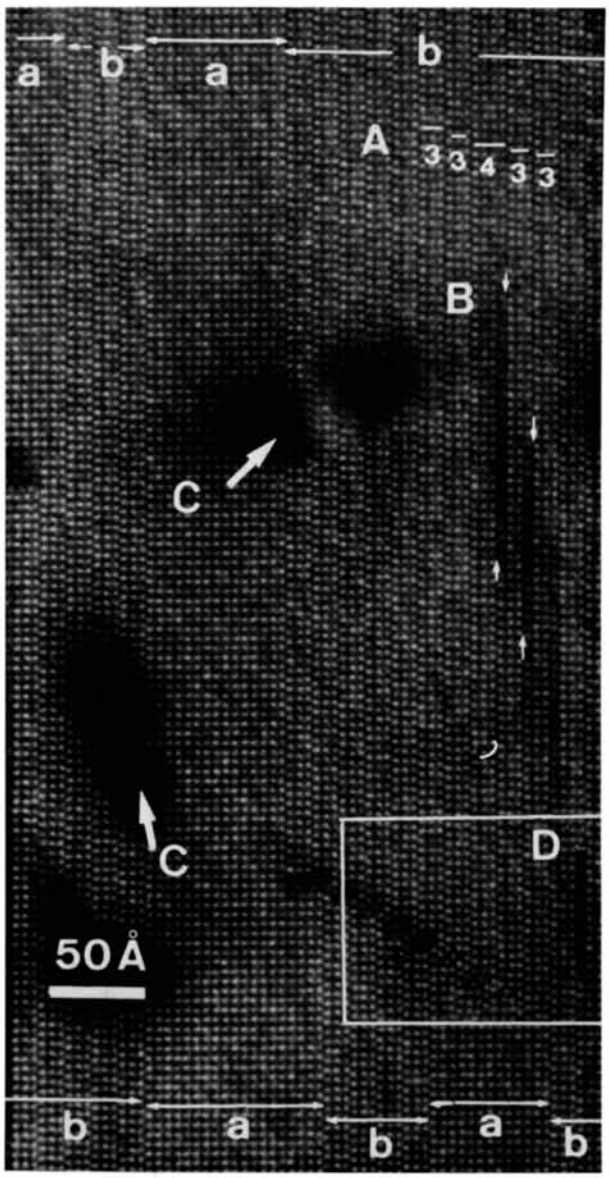

Fig. 5. Superstructure image of Au–20·7 at.% Mn, showing irregular distributions of (*A*) bright dots, (*B*) dark stripes, and (*C*) butterfly-shaped spots. The regions of the Au_4Mn and $Au_{22}Mn_6$ structures are indicated by *a* and *b*, respectively. The rectangular area (*D*) is enlarged in Fig. 6.

column and the four-dot column. At the APB, the sequential alignment of the dots changes from 343 at the top to 334 at the bottom. Note that the dots within the stripe appear to be less bright than those in the columns. This is ascribed to the statistical distribution of Mn-atom rows in the boundary, as illustrated schematically at the base of Fig. 6. According to the multislice calculation on the $D0_{22}$ structure of Au–Mn alloys, a random substitution of Au atoms in place of Mn atoms causes the brightness of the dots to decrease proportionately (Hibrabayashi, Hiraga, Shindo & Yamamoto, 1981).

Structural defects with different features are seen on the left side of Fig. 6, where misalignments occur between the ordered regions of the Au_4Mn structure at the upper and lower parts; the three-dot columns marked with white lines are shifted with respect to each other. Also note that the less-bright dots are distributed randomly at the misalignment boundary. It is assumed that this boundary is retained as an interface having an irregular distribution of the constituent atoms between the intergrown ordered regions.

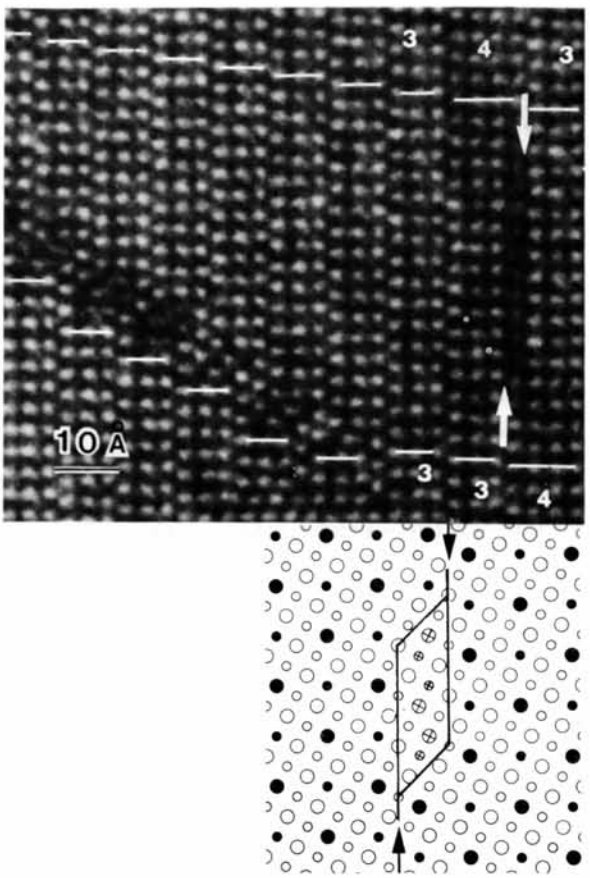

Fig. 6. Enlarged image showing structural defects in the $Au_{22}Mn_6$ structure. The vertical dark stripe indicated by arrows corresponds to the APB as illustrated by the enlarged drawing below. The misalignment boundary on the left contains a random distribution of bright dots.

In the images of Figs. 7 and 8, the Mn-atom rows appear as dark dots in contrast to the images presented above. The contrast reversal of superstructure images

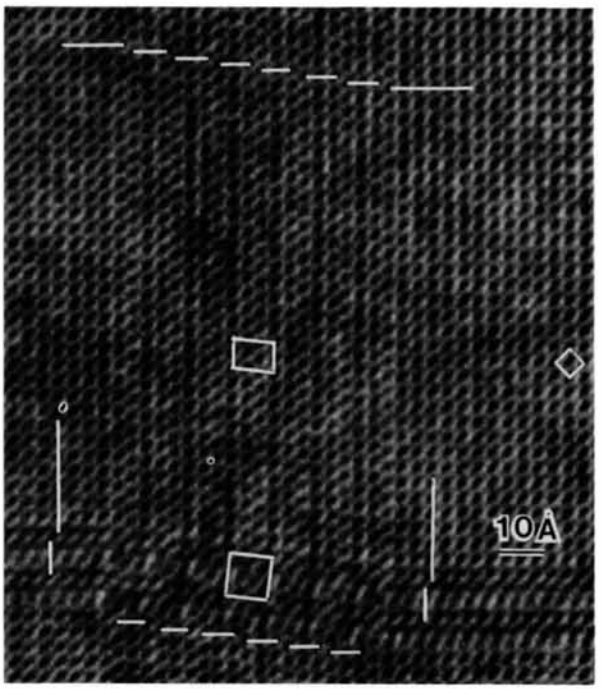

Fig. 7. Enlarged image of the outlined area in Fig. 8, showing intergrowth of the Au_4Mn, $Au_{22}Mn_6$ and $Au_{31}Mn_9$ structures. The unit cell of $Au_{31}Mn_9$ is indicated by a square.

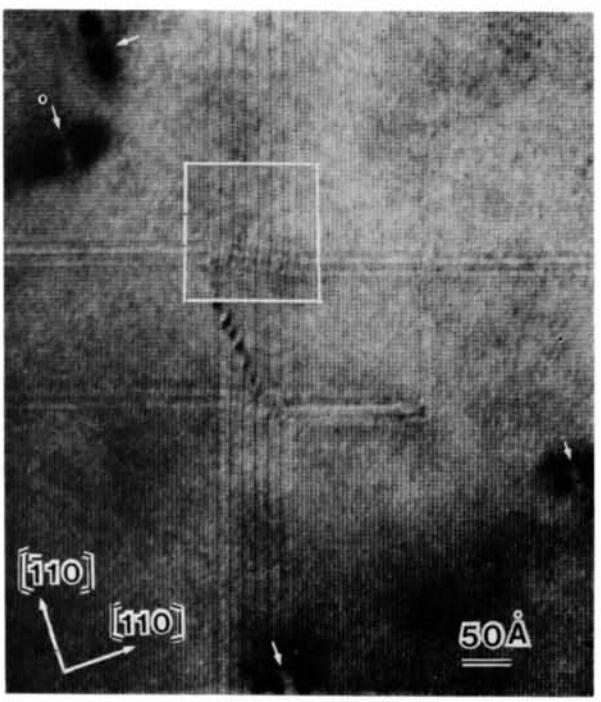

Fig. 8. Image of Au–19·5 at.% Mn, showing butterfly-shaped spots. Arrows indicate the direction of lines of no contrast.

occurs with the changes in specimen thickness and defocus (Hirabayashi, Hiraga & Shindo 1981; Hiraga *et al.*, 1981). The image of Fig. 7 shows intergrowth of the Au_4Mn, $Au_{22}Mn_6$ and $Au_{31}Mn_9$ structures, where the respective unit cells are outlined. The appearance of the $Au_{31}Mn_9$ structure is not surprising, because this structure is formed when the Au–20·7 at.% Mn alloy is annealed at 673 K as reported in part I. It is noted that the $Au_{31}Mn_9$ structure exists at intersections of the three-dot columns aligned parallel to the two orthogonal directions [210] and [1$\bar{2}$0]. This is reasonably understood because the $Au_{31}Mn_9$ structure is composed of square-shaped islands of the Au_4Mn structure and the islands are separated by 2*d*-APB along the two orthogonal directions as described in part I.

The image of Fig. 8 shows a random appearance of butterfly-shaped spots in the surrounding area of Fig. 7. These spots began to appear after electron irradiation for several hundred seconds, and grew with the irradiation time. The Mn-atom rows cannot be recognized in the dark spots, but are clearly seen along the middle lines between the paired spots. These lines are the so-called 'line of no contrast' in the image of the dislocation loops. The line of no contrast lies along the direction [110] or [$\bar{1}$10] as indicated by arrows. This is also the case in Fig. 5. The dark spots are ascribed to strain field around dislocation loops lying on {111} planes, of which the diameter is estimated as 10–30 Å. Similar dark spots have been observed in the previous study (Hirabayashi, 1980; Terasaki *et al.*, 1981).

We are grateful to Mr H. Ota and Mr E. Aoyagi for their help in the HVHREM work. The present work has partly been supported by a Grant-in-Aid for Scientific Research from the Ministry of Education, Science and Culture.

References

AMELINCKX, S. (1978–79). *Chem. Scr.* **14**, 197–206.

HIRABAYASHI, M. (1980). *Electron Microscopy*–1980, Vol. 4 (*Proceedings of the 6th International Conference on High-Voltage Electron Microscopy, Antwerp*), edited by P. BREDEROO & J. VAN LANDUYT, pp. 142–149. Leiden: Seventh European Congress on Electron Microscopy Foundation.

HIRABAYASHI, M., HIRAGA, K. & SHINDO, D. (1981). *J. Appl. Cryst.* **14**, 169–177.

HIRABAYASHI, M., HIRAGA, K., SHINDO, D. & YAMAMOTO, T. (1981). *Sci. Rep. Res. Inst. Tohoku Univ. Ser. A*, **29**, Suppl. 1, 1–6.

HIRAGA, K., SHINDO, D. & HIRABAYASHI, M. (1980). *Electron Microscopy*–1980, Vol. 4 (*Proceedings of the 6th International Conference on High-Voltage Electron Microscopy, Antwerp*), edited by P. BREDEROO & J. VAN LANDUYT, pp. 170–173. Leiden: Seventh European Congress on Electron Microscopy Foundation.

HIRAGA, K., SHINDO, D. & HIRABAYASHI, M. (1981). *J. Appl. Cryst.* **14**, 185–190.

HIRAGA, K., SHINDO, D., HIRABAYASHI, M., TERASAKI, O. & WATANABE, D. (1980). *Acta Cryst.* B**36**, 2550–2554.

TERASAKI, O., WATANABE, D., HIRAGA, K., SHINDO, D. & HIRABAYASHI, M. (1980). *Micron*, **11**, 235–240.

TERASAKI, O., WATANABE, D., HIRAGA, K., SHINDO, D. & HIRABAYASHI, M. (1981). *J. Appl. Cryst.* **14**, 392–400.

VAN TENDELOO, G. (1980). *J. Microsc. (Oxford)*, **119**, 125–140.

WATANABE, D. (1957). *Acta Cryst.* **10**, 483–485.

WATANABE, D. (1979). *Modulated Structures*–1979, *AIP Conf. Proc.* No. 53, edited by J. M. COWLEY, J. B. COHEN, M. B. SALAMON & B. J. WUENSCH, pp. 229–239. New York: American Institute of Physics.

Acta Cryst. (1982). A**38**, 274–285

Symmetrized Multipole Analysis of Coupled Orientation–Translation Distributions

BY MIKKO KARA

Department of Physics, University of Helsinki, Siltavuorenpenger 20 *D, SF*-00170 *Helsinki* 17, *Finland*

(*Received* 28 *May* 1981; *accepted* 26 *October* 1981)

Abstract

Symmetrized multipole formalism, in diffraction studies of orientationally disordered molecular crystals, is generalized to include coupling between orientations and translations of a rigid body and anharmonicity in the center-of-mass motion. This generalized formalism is intended for use with direct multipole analysis of the observed form factors. In the relationships between the radial multipole coefficients of the dynamic and static density, correlations cause a mixing in the multipole order. In the dynamic form factor the parameters describing the coupling are linear combinations of the multipole expansion coefficients of the corresponding rigid-body distribution. Parameters describing anisotropy are directly the multipole expansion coefficients

0567-7394/82/020274-12$01.00